

Effective Activation Energy for the Solid-State Sintering of Silicon Carbide Ceramics



DULAL CHANDRA JANA, G. SUNDARARAJAN, and K. CHATTOPADHYAY

Effective activation energy for densification of SiC in the presence of C and B₄C additives is determined by constant heating rate experiments through analysis of shrinkage in hot pressing. The activation energy (AE) for sintering increased linearly with the relative density (RD) in two different regimes. The effective AE increased from 407 ± 50 kJ/mole at 75 pct RD to 1132 ± 75 kJ/mole at 95 pct RD. Lattice diffusion is proposed as the predominant mechanism for SiC densification at higher density. This is also validated by the uniform distribution of sintering additive through electron probe microanalysis. The low AE in the regime of lower density could be attributed to the pressure-assisted particle rearrangement during hot pressing. The relative contribution of both the mechanisms between two density limits resulted in the change in AE for sintering. The mechanisms of defect generation resulting in densification are also discussed.

<https://doi.org/10.1007/s11661-018-4884-9>

© The Minerals, Metals & Materials Society and ASM International 2018

I. INTRODUCTION

SILICON carbide (SiC) is a material of immense technological importance as it exhibits outstanding properties including light-weight, high strength, moderate toughness, high wear, and oxidation resistance and strength retention at elevated temperature.^[1,2] SiC is suitable for various applications including the main structural material in telescopes for space exploration, as abrasives for cutting and grinding, in wear parts such as bearings and atomization nozzles, for the production of seals and valves for demanding chemical environments in the process industry, high-temperature heat exchangers and in ceramic armor plates for ballistic protection.^[1-3] Because of the high melting point and brittle behavior of SiC, normal melting and deformation processes are not suitable for the shaping of SiC components. Therefore, SiC components for various applications are produced by powder consolidation techniques involving shape formation followed by temperature-assisted densification.

SiC is difficult to sinter in the absence of sintering additives and/or external pressure.^[4] The lack of

inherent sinterability of SiC is due to the presence of covalent chemical bonds in it. The kinetic and thermodynamic phenomena associated with the non-sinterability can also be explained based on its strong and directional covalent bonding. The activation energy (AE) for Si and C diffusion in pure SiC is very high due to the high energy involved in the formation and movement of structural defects.^[5] A powder compact undergoes densification and appreciable shrinkage is noticed only when the mass transfer occurs at the pore surfaces through volume or grain boundary diffusion during heat treatment at elevated temperatures. In contrary, the presence of other mass transfer mechanisms of low AE (*e.g.*, surface diffusion and evaporation/condensation) by which material transport can occur from pore surfaces to the neck can lead to a reduction of the specific surface area through particle coarsening. Under these conditions, very little shrinkage or densification are observed.^[4] Conventionally, SiC can be densified in the absence of sintering aids by pressure-assisted densification processes like hot pressing (HP) and hot isostatic pressing (HIP). However, pressure-assisted densification processes are limited to the fabrication of simple parts and not economical for mass production.

SiC components can also be made either by reaction bonding process or densification in the presence of additives including C and B as solid-state sintering additives and Y₂O₃/Al₂O₃ as liquid-phase sintering additives. However, the SiC parts sintered in the presence of C and B additives possess advantages in terms of their homogenous microstructure and superior strength at elevated temperatures compared to that of liquid-phase sintered or reaction bonded SiC.^[6,7] The

DULAL CHANDRA JANA is with the Centre for Non-Oxide Ceramics, International Advanced Research Centre for Powder Metallurgy & New Materials (ARCI), Balapur PO, RCI Road, Hyderabad 500 005, India. Contact e-mail: janad@arci.res.in. G. SUNDARARAJAN is with the Centre for Non-Oxide Ceramics, International Advanced Research Centre for Powder Metallurgy & New Materials (ARCI) and also with the Metallurgical and Materials Engineering, Indian Institute of Technology, Madras, Chennai, India. K. CHATTOPADHYAY is with the Department of Materials Engineering, Indian Institute of Science, Bangalore 560 012, India.

Manuscript submitted March 27, 2018.

Article published online August 30, 2018

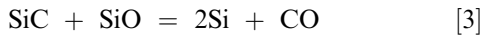
non-homogenous microstructure in the liquid-phase sintered SiC (LP-SiC) is attributed to the Al₂O₃ evaporation, SiC decomposition and weight loss resulting in the formation of Y₂O₃ rich phases. Prochazka^[8] first reported that sub-micron size β-SiC can be densified in the absence of any secondary phase by pressureless sintering through the concurrent addition of 0.4 wt pct of B and 0.5 wt pct of C as the additives. The author concluded that C reduced SiO₂ on SiC particles and B segregation at the grain boundaries with the reduction of grain boundary energy enhanced the densification.

From the thermodynamic viewpoint, the driving force for sintering is the difference between solid-vapor surface energy (γ_{sv}) and grain boundary energy (γ_{gb}). It was proposed that the high ratio between γ_{gb} and γ_{sv} in SiC prevents the densification. Considering a pore located in the grain boundary triple point, the relationship between these two surface energies can be given by^[4]

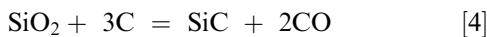
$$\gamma_{gb} = 2\gamma_{sv}\cos\frac{\theta}{2}, \quad [1]$$

where θ is the dihedral angle. Therefore, pore shrinkage and densification would occur only when the $\theta > 60$ deg or $\gamma_{gb}/\gamma_{sv} < \sqrt{3}$. Thus, the overall decrease of γ_{gb}/γ_{sv} enhances the densification.^[8] However, the exact role of C and B in mass transport mechanisms for sintering has not been fully understood.

As far as the role of C is concerned, earlier studies suggest that in the absence of carbon the decomposition of SiC is promoted by the SiO₂ layer on SiC particles as per the following reaction.^[9,10]



These reactions inhibit sintering due to the formation of gaseous species and also result in particle coarsening with the development of a network of large pores through enhanced surface diffusion of free Si. Conversely, the presence of sufficient C prevents the decomposition of SiC at elevated temperature as per the following reaction^[9]:



Thus, C as sintering additive prevents the decomposition of SiC and also modifies the sintering kinetics by reducing the rate of vapor phase mass transport e.g., surface diffusion and evaporation/condensation. These explanations are in agreement with the role of C as proposed by Prochazka.^[8] However, the weight loss vs temperature study^[10] shows the reaction (Eq. [4]) which prevents the SiC decomposition occurs in the temperature range 1200 °C to 1675 °C, well below the onset of densification. Therefore, the role of C in the enhancement of densification remains unexplained.

Lange and Gupta^[11] reported transient liquid-phase sintering in SiC in the presence of C and B as the additives. The presence of liquid phase during the densification of the nano-SiC particle by spark plasma sintering (SPS) is also reported.^[12] The postulate of transient liquid-phase sintering is supported by the phase diagram reported by Keiffer *et al.*^[13] which shows the appearance of the liquid phase in the ternary B-C-Si system at 2150 °C. However, SiC can be sintered higher than 90 pct RD in the presence of C and B by maintaining the densification temperature below 2100 °C. The densification of SiC through activation of grain boundary^[14] as well as lattice diffusion^[15] is also reported in the literature.

In this work, we attempted to predict the densification mechanism of SiC in the presence of solid-state sintering additives (C and B₄C) by determining the AE through constant heating rate (CHR) experiments at constant load. CHR experiments were carried out in a hot-press to obtain the densification data from the shrinkage of the specimen. The sintering model of Wang and Raj^[16] is applied for analysis of densification data. According to this model, the densification rate ($\dot{\rho}$) at a constant load that depends on the temperature, grain size, and density is expressed as

$$\dot{\rho} = \frac{d\rho}{dt} = A \frac{\exp(-Q/RT)f(\rho)}{T d^n}, \quad [5]$$

where

$$A = \frac{C\gamma V^{2/3}}{R}. \quad [6]$$

In these expressions, Q is the AE; R is the universal gas constant; T is the absolute temperature, and d is the grain size. The function $f(\rho)$ depends on density only and n is known as the grain size exponent which depends on the mechanism of densification (n can be either 3 or 4 depending on the densification is controlled by either lattice diffusion or grain boundary diffusion, respectively). A is a material parameter that is related to the surface energy (γ) and molar volume (V) in accordance with Eq. [6] while C is a constant. The rate of densification ($\dot{\rho}$) *i.e.*, the time rate of density change is expressed as

$$\dot{\rho} = \frac{d\rho}{dt} = \frac{d\rho}{dT} \frac{dT}{dt} = \frac{d\rho}{dT} \dot{T}, \quad [7]$$

where \dot{T} is the rate of heating, kept constant during the experiment. The combination of Eqs. [5] and [7] and applying logarithms yield that

$$\ln\left(T\dot{T}\frac{d\rho}{dT}\right) = -\frac{Q}{RT} + \ln[f(\rho)] + \ln A - n \ln d. \quad [8]$$

The activation energy (Q) can be obtained from Arrhenius-type $\ln\left(T\dot{T}\frac{d\rho}{dT}\right)$ vs $1/T$ plot with the assumption that the density (ρ) and grain size (d) remain constant. In CHR experiments, the density values are obtained with increasing value of temperature when the

specimen is heated at a specified rate of rising of temperature. The density vs temperature profile shows sigmoidal behavior. The sintering rate increases rapidly with the increase of temperature followed by gradually fall when the specimen achieves the higher density. Eventually, the sintering rate falls to zero as the specimen achieves its full density. The sigmoidal density profile shifts to a higher temperature when the sintering experiments are carried out at a higher heating rate. Therefore, sintering rate at same density but at different temperatures can be obtained by carrying out several sets of sintering experiments at different heating rates.

The changes in grain size during sintering experiments lead to complications in determining the AE. Wang and Raj^[17] described several approaches to accommodate the grain size correction in determining the AE. One of the approaches relies on the facts that the density and grain size are related by a phenomenological correlation. In the regime of densification, the grain size of a sintered specimen does not depend on the sintering pathways (*e.g.*, temperature, heating rate *etc.*) but only on density provided that same initial green state is maintained. It is shown in our study that grain size and density data are in accordance with this correlation. Therefore, the grain size term in Eq. [8] is accommodated in the density function $f(\rho)$ and the estimate of AE as per Eq. [8] corresponds to a given combination of density and grain size which is termed as the effective AE. Based on the estimates of AE in this study, we propose the possible mass transport mechanism for solid-state sintering of SiC and validate by mapping of elemental boron through electron probe microanalysis (EPMA).

II. EXPERIMENTAL PROCEDURE

A. Raw Material and Methods

Commercial grade α -SiC powder (Densitac 15) of Saint-Gobain Ceramic Materials, Norway was used for the studies. Densitac 15 is a spray dried premix SiC powder and it contains approximately 3.0 wt pct C in the form of phenolic resin and 1 wt pct B₄C as the sintering additives. Impurities content in the powder were 0.75 wt pct of SiO₂, 0.005 wt pct of free Si in addition to the 0.20 wt pct of free C, and 0.85 wt of pct total O. The powder was hot pressed at 10 MPa and a constant rate of heating was applied to raise the temperature. Typically, 150 g powder was placed in a graphite die lined with thin graphite foil to prepare SiC billets of approximate size 100 mm × 100 mm × 5 mm. The temperature of the hot press (Advanced Vacuum System Inc., USA) was raised to 1500 °C at a rate of 10 °C/min and then waited for 10 minutes. Subsequently, different heating rates 2.5, 3.75, 5.0, and 7.5 °C/min were applied to increase the temperature to 2100 °C. The experiments were performed in an argon atmosphere and then terminated when the temperature reached 2100 °C. The details of CHR experiments through hot pressing are described elsewhere.^[18]

The shrinkage of the specimen (Δl) in our experiment was measured by recording the position of hot press ram

monitored by an optical linear encoder. Since the cross section of the specimen remained unchanged during hot pressing, the density (ρ) of the specimen as a function of temperature was estimated as per the following equation:

$$\rho = \rho_f \left(\frac{l_f}{l} \right) = \rho_f \left(\frac{l_f}{l_0 - \Delta l} \right), \quad [9]$$

where l_f is the final thickness of the specimen; l is the thickness during hot pressing, and ρ_f is the final density as measured by the Archimedes principle. The shrinkage data were collected in the temperature range of 1600 °C to 2100 °C at an interval of every 10 °C. For the estimation of specimen density at 1600 °C, l_0 was considered as the sum l_f and total shrinkage for the increase of temperature from 1600 °C to 2100 °C. In order to obtain reliable data, the expansion of graphite ram was calibrated by conducting a minimum of three identical experiments without SiC powder. Relative densities (RD) were obtained by dividing the density data with the theoretical density of SiC (3.21 g cm⁻³).

B. Material Characterizations

The bulk density of sintered specimens (ρ_f) was measured by Archimedes principle (ASTM C372) with the help of Sartorius balance (CP 225D, AG Gottingen, Germany) as per the following equation:

$$\rho_f = \frac{W_d}{W - S} \quad [10]$$

where W_d is the dry weight; W is the soaked weight, and S is the suspended weight of the specimen using deionized water as the immersion medium. Microstructural analysis of SiC powder and sintered specimens were performed using a Hitachi make model S-3400N scanning electron microscope (SEM) employing secondary electron imaging mode. For the determination of grain size, sintered specimens were sectioned and polished up to 1 μ m diamond grit and thermally etched at 1450 °C under argon atmosphere. The average grain was estimated through perimeter measurement method of around 300 grains on polished and etched micrographs. An electron probe micro analyzer (JEOL JXA-8530F) was used for determining boron map on the polished surfaces of sintered SiC. The instrument is equipped with field emission electron gun, six wavelength dispersive X-ray spectrometers (WDS), and an energy-dispersive X-ray spectrometer (EDS). The instrument can simultaneously analyze three elements through WDS and sixteen elements through EDS along with forming of both backscatter and secondary electron images.

III. RESULTS

A. Raw Material Characteristics

The raw SiC powder used in our study consists of spray dried granules. The size morphology of these granules is shown in Figure 1(a). Also, the size of the

granules from the figure is found to be in the ranges of 10 to 80 μm . However, each of the spray dried granules contains smaller size primary particles that are shown in Figure 1(b). The average size of the primary particles from perimeter measurement is observed to be about 1 μm .

B. Densification

The plot of density vs temperature in CHR experiments for different heating rates is presented in Figure 2. As seen from the figure, rapid change in density is observed above 1800 $^{\circ}\text{C}$ which could be considered as the onset of densification. Further, at a given temperature, higher RD is observed for lower applied heating rates as the specimen experiences longer dwell time at a given temperature for lower heating rate before it reaches to the next higher temperature. The RD vs temperature curve shows sigmoidal behavior for slower heating rates (e.g., 2.5 and 3.75 $^{\circ}\text{C}/\text{min}$) where the densification rate increases rapidly with temperature after the onset of the densification followed by a reduction as the specimen achieves higher density. The falling tail in the sigmoidal curves could not be noticed for higher heating rates (e.g., 5.0 deg and 7.5 $^{\circ}\text{C}/\text{min}$) in the temperature range of our study due to the delayed densification.

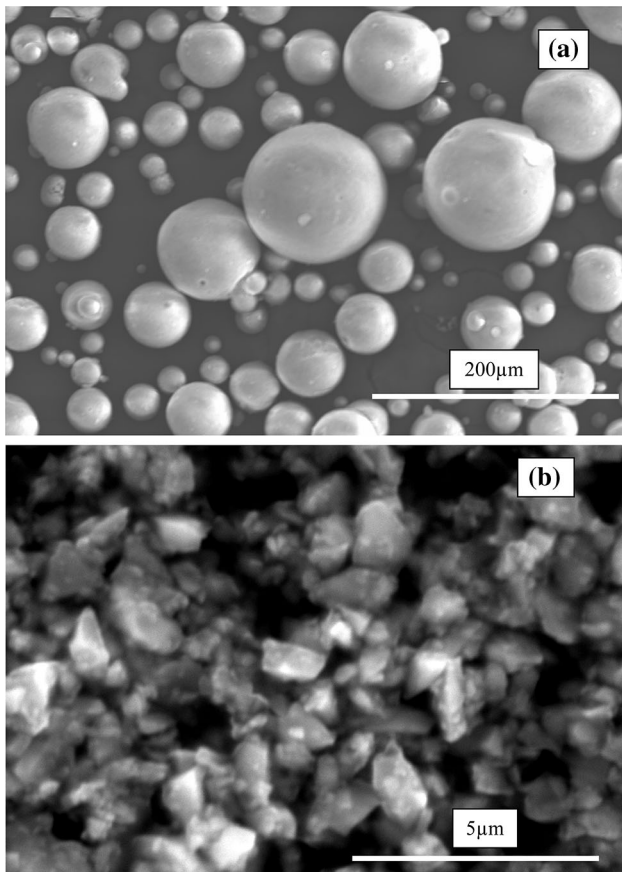


Fig. 1—SEM micrograph of (a) spray dried granules and (b) primary particles.

The plot of $d\rho/dT$ vs temperature in Figure 3 passes through a maxima at lower heating rates. Also, the increase of heating rate shifts the maxima to a higher temperature along with the increase in the height of the maxima due to the delayed densification. The $d\rho/dT$ vs temperature plot at higher heating rates (5.0 deg and 7.5 $^{\circ}\text{C}/\text{min}$) could not reach the maxima (Figure 3) which is consistent with the absence of falling tail in the density profiles (Figure 2).

C. Master Sintering Curve

The average grain size of SiC specimens with different RD ranging between 68 and 99 pct is shown in Figure 4. Each data point (grain size and RD) in Figure 4 corresponds to a given combination of sintering temperature and heating rates. While preparing the different RD samples, sintering temperature was varied between 1900 $^{\circ}\text{C}$ and 2100 $^{\circ}\text{C}$. The heating rates were varied independently to reach the target temperature and applied heating rates were 2.5, 5.0, and 7.5 $^{\circ}\text{C}/\text{min}$. As for example, SEM micrograph of 0.99 RD specimen in

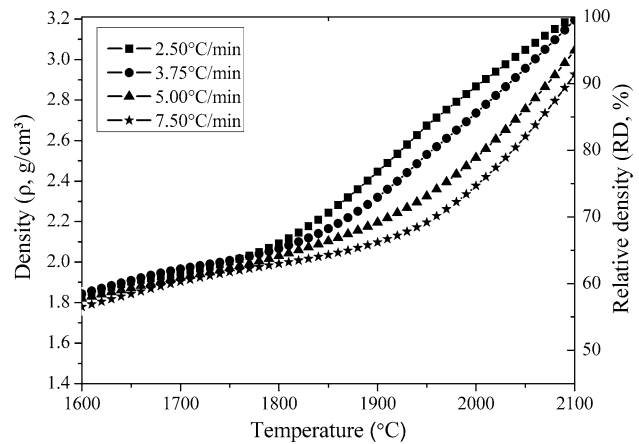


Fig. 2—Density vs temperature curves in the CHR experiments with different heating rates.

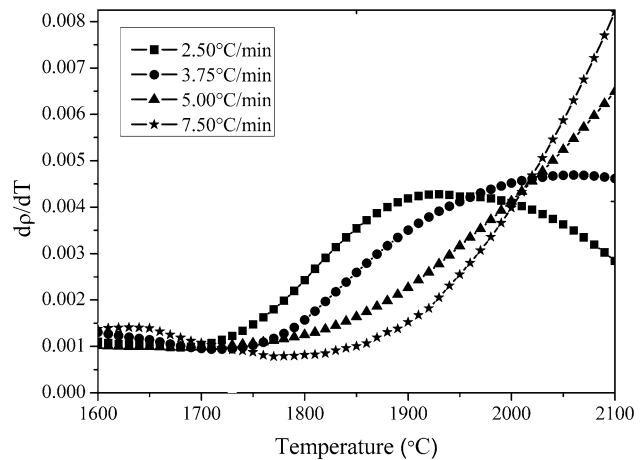


Fig. 3—Temperature derivative of density vs temperature curves for the CHR experiments with different heating rates.

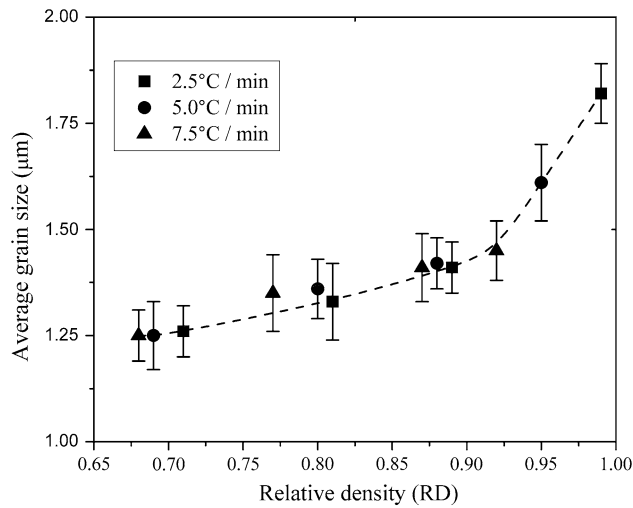


Fig. 4—Average grain size vs RD of SiC follows the master sintering curve (MSC).

Figure 5(a) corresponds to the 2100 °C sintering temperature and the heating rate of 2.5 °C/min. Two other representatives SEM micrographs with the sintering temperature 2100 °C are shown in Figures 5(b) and (c) with the applied heating rates of 5.0 and 7.5 °C/min, respectively. The average grain size of different RD specimens as indicated in Figure 4 was determined from the SEM micrographs by perimeter measurement method. A moderate increase in grain size from 1.25 to 1.82 μm is observed in Figure 4 as the RD increases from 68 to 99 pct in comparison to the 1 μm particle size in the starting powder. Irrespective of the final sintering temperature and heating rate, the grain size vs RD data belong to the similar trend, commonly known as the master sintering curve (MSC, dashed line in Figure 4).

There are several factors that control the densification along with microstructural evolution in ceramics.^[19] The material parameters that control the densification include powder characteristics (e.g., purity, particles size, morphology), composition and sintering additives. Additionally, various sintering parameters including temperature, soaking time, the rate of heating and sintering environment also affect the sintering. In spite of these, a phenomenological correlation exists where the grain size is a function of only the RD provided that same powder-additive composition and process are used to make the green body.^[17,19] Grain size results of our study also indicate that irrespective of different sintering parameters (temperature, heating rate etc.) constant grain size can be assumed once the RD is specified. Therefore, Eq. [8] can be applied to estimate the effective AE.

The MSC model for sintering of ceramics i.e., correlation between density and grain size holds well during the progress of densification. However, the model fails when the extent of densification approaches to the near theoretical density as the grain size of sintered materials with 100 pct RD could be different through the variation of holding time.

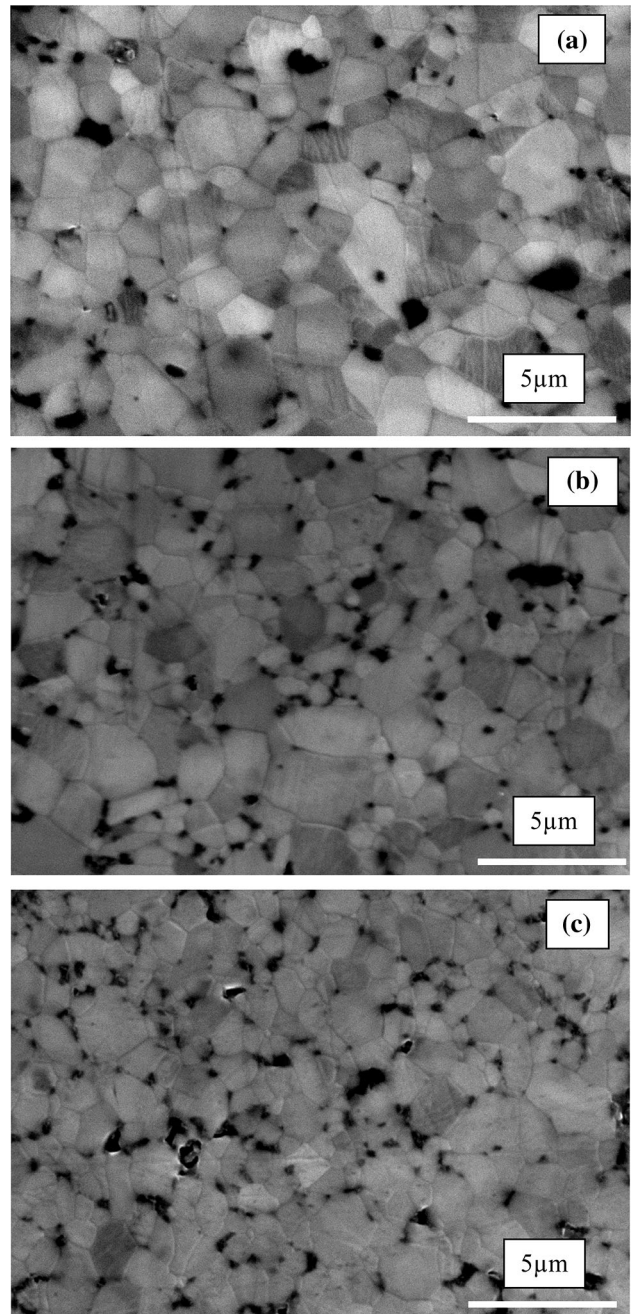


Fig. 5—SEM micrographs of SiC with different RD obtained by heating up to 2100 °C with different heating rates (HR): (a) HR = 2.5 °C/min, RD = 0.99 and average grain size (d_{50}) = 1.82 μm, (b) HR = 5.0 °C/min, RD = 0.95 and d_{50} = 1.61 μm and (c) HR = 7.5 °C/min, RD = 0.92 and d_{50} = 1.45 μm.

D. Effective AE for Densification

The Arrhenius-type $\ln\left(T\dot{T}\frac{d\rho}{dT}\right)$ vs $10^4/T$ plot for different RD is shown in Figure 6 and the slope of the plot corresponds to the AE. As the Arrhenius-type plots for different RD are not parallel indicating the changes of AE with the RD. For the sake of clarity, the variation of AE with RD is shown in Figure 7. It is observed from the figure that the AE increases almost linearly from 407 ± 50 kJ/mole at 75 pct RD to 1132 ± 75 kJ/mole at 95

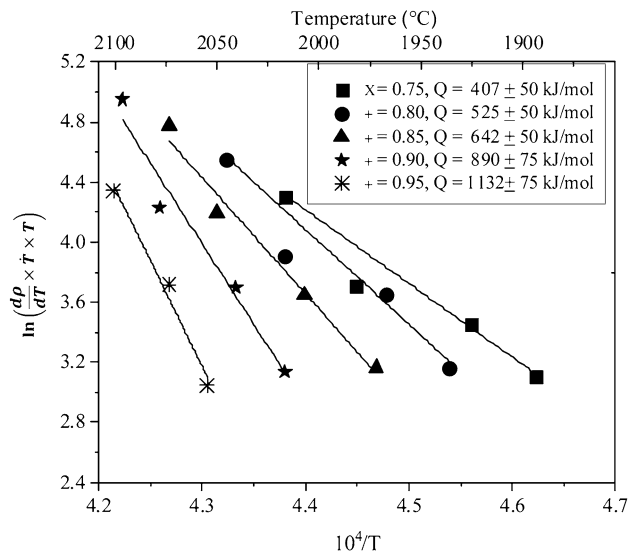


Fig. 6—Arrhenius-type plot of $\ln\left(T\dot{T}\frac{dp}{dT}\right)$ vs $10^4/T$ for the estimation of effective AE for sintering of SiC.

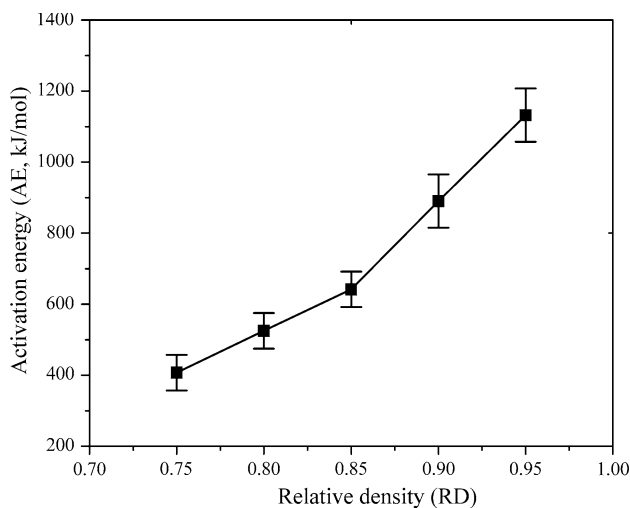


Fig. 7—The variation of effective AE with RD for sintering of SiC.

pct RD in two different regimes that are separated at about 85 pct RD. Also, the increase of AE with RD below 85 pct is seen to be slower compared to the increase of AE above 85 pct RD.

E. Electron Probe Microanalysis (EPMA)

The distribution of various elements in the sintered specimens was investigated by EPMA where the concentrations of light elements (B, C, and O) were determined by WDS compared to the Si concentration through EDS. The mapping of B and total elements (sum of Si, C, O, and B) are shown in Figure 8 with reference to the BSE micrograph of SiC having 99 pct RD. The BSE micrograph [Figure 8(a)] consists of randomly distributed SiC grains along with few localized dark regions (due to the low BSE yield). The distribution of B in Figure 8(b) is seen to be uniform

except for some localized regions with highly intense B signals. It could be predicted from the uniform B distribution that B enters into the SiC lattice through the formation of a solid solution.

Careful observation reveals two types of dark regions embedded in the matrix. The boundary of first category dark regions shows a sharp contrast with the matrix which could be attributed to the excess of sintering additives^[20] (low atomic mass B and C resulted from low BSE yield). The other type shows defocused boundary with the matrix due to the residual porosity in the specimen. Therefore, the signals from the localized region are could be associated with the excess of B than its solubility in SiC crystal or/and due to the artefact from the regions with low atomic mass or porosity [as the wt pct of total elements in the dark regions exceeds about 400 pct or more in Figure 8(c)].

IV. DISCUSSIONS

Following the results presented in the previous section, we can summarize that the effective AE increases linearly from 407 ± 50 kJ/mole at 75 pct RD to 1132 ± 75 kJ/mole at 95 pct RD in two different regimes. The density-dependent AE in sintering of SiC has not been reported in the earlier literature. The changes in AE with density in sintering of yttria-stabilized zirconia (YSZ) are reported by Bernard-Granger and Guizard^[21] where apparent AE decreased from 935 kJ/mole at 70 pct RD to 310 kJ/mol at 90.9 pct RD. Normally, the AE remains same with the increase in density during sintering^[16,18] since a given value of AE is tied to a particular mechanism. The gradual change in AE does not mean that each step of density increase is associated with different mechanisms. Bernard-Granger and Guizard explained the gradual changes in AE based on two types of mechanisms involved and their relative contribution. They considered that the apparent AE is the sum of energy terms associated with the point defect formation and the other terms related to the grain boundary diffusion. Accordingly, the high AE 935 kJ/mole at 70 pct RD is due to the difficulty in creating point defects when the pores are not closed. Conversely, at higher RD point defect formation is easy and the low AE 310 kJ/mole at 90.9 pct RD is merely the AE for grain boundary diffusion.

The effective AE 1132 ± 75 kJ/mole at 95 pct RD obtained in our study could be associated with lattice diffusion as Hong *et al.*^[22] reported AE for lattice diffusion for Si and C in β -SiC are 912 ± 5 and 841 ± 14 kJ/mol, respectively. The estimate of higher AE than that available from atomic diffusion data may be due to the effect of heating rate. In CHR experiments, lower heating rates result in specimens dwelling longer at lower temperature.^[23] The densification in these cases is inhibited by surface diffusion. The retarding effect of surface diffusion resulted in a higher AE than the actual. Further, the limitation in the measurements of specimen temperature (inside die cavity) leads to an error in the estimated effective AE.

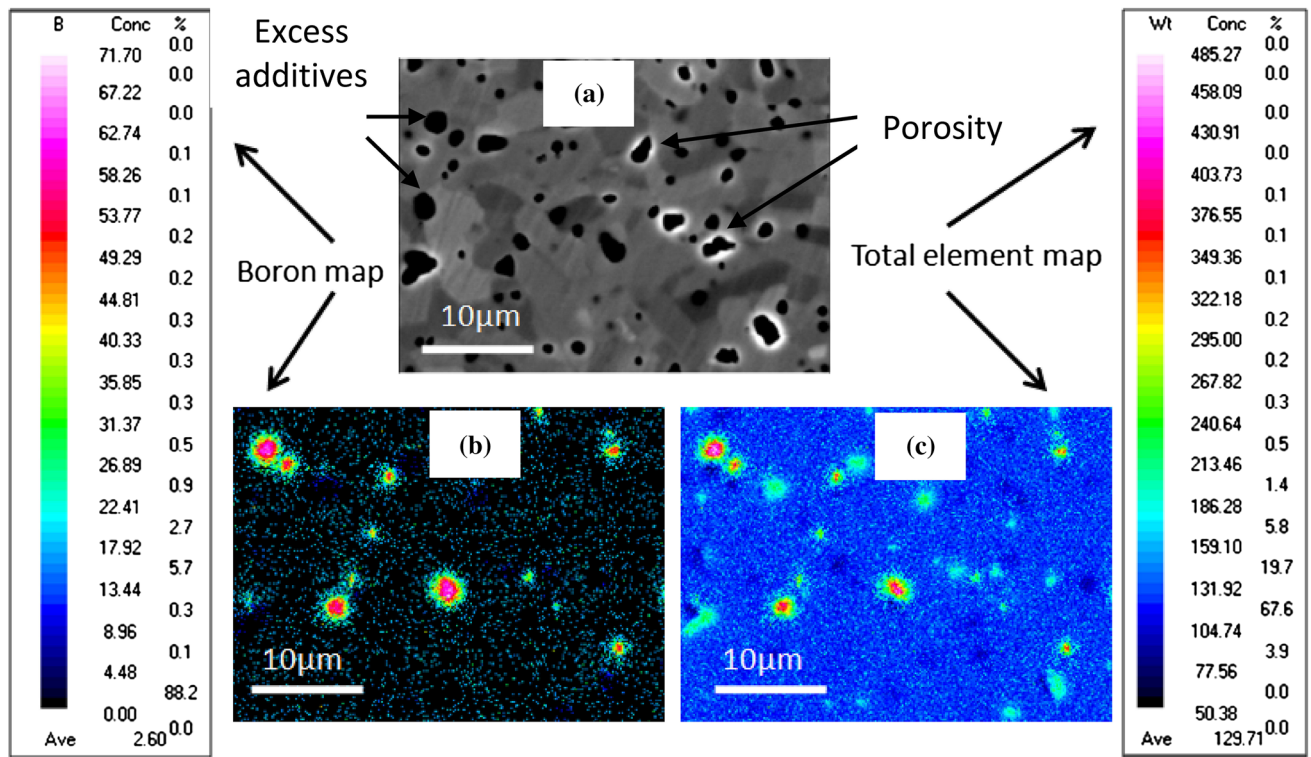


Fig. 8—Electron probe microanalysis results: (a) BSE micrograph of SiC with relative density 0.99, (b) distribution map of B and (c) distribution map of total elements (C, Si, B and O).

The occurrence of low effective AE 407 ± 50 kJ/mol at 75 pct RD (which is less than the AE either for lattice or grain boundary diffusion) is not clear to us and it requires further investigation. Wilkinson and Ashby reported^[24] that the densification under pressure is the combined effect of many mechanisms including diffusion, particle rearrangement, plasticity etc. The low effective AE at 75 pct RD could be attributed to the pressure-assisted mechanisms including particle sliding and particle rearrangement since AE is estimated in the presence of external pressure 10 MPa.

Hence, we propose that the sintering of SiC in the presence of external pressure is the combined effect of two mechanisms. When the body consists of interconnected pores at low RD (Stage II sintering) the densification occurred with the assistance of external pressure and low effective AE is observed. In contrary, the effect of external pressure (10 MPa) in the final stage of sintering (specimens consists of isolated pores) is negligible and lattice diffusion is appeared to the predominant mechanism by resulting in the effective AE 1132 ± 75 kJ/mol at 95 pct RD. Between these two RD limits, either of the mechanisms contributes to an emergence of an effective AE.

Sintering of SiC through activation of lattice diffusion in the presence of C and B_4C additives has been suggested by several investigators. Datta *et al.*^[15] reported that B can substitute Si atom in SiC and enhances the lattice diffusion. van Rijswijk and Shane-field^[9] reported that higher Si diffusion coefficient in C atmosphere favors the densification through bulk

diffusion. Microanalytical analysis of sintered SiC by high-resolution Auger electron spectroscopy (HRAES)^[25] indicates the absence of B enrichment at the grain boundaries that also support B incorporation in SiC lattice. Therefore, uniform distribution of B from EPMA results and high effective AE of our study are in agreement with lattice diffusion for densification of SiC.

The role of C and B from B_4C in influencing lattice diffusion is discussed below. The intrinsic C and Si vacancy concentration in pure SiC can be expressed as follows^[26]:

$$n_C = N \exp(-\Delta H_C/kT) \quad [11]$$

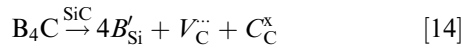
$$n_{Si} = N \exp(-\Delta H_{Si}/kT) \quad [12]$$

$$n_C \cdot n_{Si} = N^2 \exp[-(\Delta H_C + \Delta H_{Si})/kT], \quad [13]$$

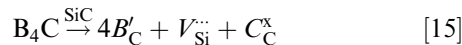
where N is the total number of atomic sites; n is the number of vacant sites; ΔH is the enthalpy associated with vacancy generation; k is the Boltzmann constant, and T is the absolute temperature. As shown in Eq. [13] the product of vacancy concentration of C and Si ($n_C \cdot n_{Si}$) is constant as far as the temperature remains unchanged. The vacancy concentration of C and Si in SiC lattice will vary depending on the partial pressure of constituents in the surrounding atmosphere. Therefore, a C-rich atmosphere would enhance the Si diffusion and suppresses C diffusion and vice versa. The increase in Si diffusion coefficient in C atmosphere is reported.^[9,27]

As far as the role of B in the form of B₄C is concerned, one can argue that defects associated with B-SiC solid solution increase the lattice diffusion of both C and Si resulting in densification of SiC.^[28] The solid solubility of B and its site occupancy in SiC lattice are well reported.^[29,30] Sridhara *et al.*^[31] reported that B can act as a shallow dopant with ionization energy 0.30 eV or deep dopant with ionization energy 0.65 eV when it occupies Si or C sites, respectively. Depending on the ionization energy (IE) and site occupancy of B in SiC lattice, we propose the following defect reactions:

B in Si site for IE = 0.30 eV:



B in C site for IE = 0.65 eV:



The concentration of ionized B defects (n_{B}) in substituted SiC lattice can be expressed as

$$n_{\text{B}} = C_1 N_{\text{B}} \exp(-E_{\text{d}}/kT), \quad [16]$$

where C_1 is a constant; N_{B} is the B concentration in the substituted lattice, and E_{d} is the IE. When SiC sintering temperature is about 2000 °C, the kT energy equivalent is approximately 0.20 eV which is comparable with the ionization energy of B as the shallow dopant. As a result of that significant proportion B in the shallow energy state will generate defects as per Eq. [14]. The occurrence of lattice defects increases the atomistic of diffusion and hence the diffusion coefficient.^[25,32,33] In particular, if the solute atom is accompanied by a vacancy (Eq. [14]), the solute atom always has an adjacent site to jump. As a result of that, solute diffusion coefficient increases to the order of vacancy diffusion coefficient. Therefore, the presence of C and B enhances the densification of SiC through activation of lattice diffusion.

V. CONCLUSIONS

Sintering kinetics of SiC at constant pressure is investigated through analysis of densification data as obtained from CHR experiments. The grain size measurement results show that grain size is a function of the only RD when the same green state and powder composition are maintained. Thus, the effective AE can be estimated for given combinations of RD and grain size. The low effective AE 407 ± 50 kJ/mol is observed at 75 pct RD could be associated with the pressure-assisted mechanisms. The high AE of 1132 ± 75 kJ/mol at 95 pct RD is associated with the process of densification predominately through lattice diffusion. The change in effective AE with RD occurred due to the change in the relative contribution of these two mechanisms. Uniform B distribution as revealed by EPMA experiments confirms the incorporation of B in

SiC lattice. Hence, the defects associated with B incorporation enhanced lattice diffusion and the densification.

REFERENCES

1. K. Yamada and M. Mohri: in *Silicon Carbide Ceramics-1: Fundamentals and Solid Reaction*, S. Somiya and Y. Inomata, eds., Elsevier Applied Science, New York, 1991, pp. 13–44.
2. H. Tanaka: *J. Ceram. Soc. Jpn.*, 2011, vol. 119, pp. 218–33.
3. M. Flinders, D. Ray, A. Anderson, and R.A. Cutler: *J. Am. Ceram. Soc.*, 2005, vol. 88, pp. 2217–26.
4. C. Greskovich and J.H. Rosolowski: *J. Am. Ceram. Soc.*, 1976, vol. 59, pp. 336–43.
5. V.A. Bron: *Sov. Powder. Metall. Met. Ceram.*, 1975, vol. 54, pp. 339–44.
6. J.J. Melendez-Martinez, M. Castillo-Rodriguez, and A. Dominguez-Rodriguez: *J. Am. Ceram. Soc.*, 2007, vol. 90, pp. 163–69.
7. J.F.A. Munoz, A.R.A. Lopez, F.M.V. FERIA, A.D. Rodriguez, and M. Singh: *Acta Mater.*, 2003, vol. 51, pp. 3259–75.
8. S. Prochazka: The Role of Boron and Carbon in Sintering of Silicon Carbide in *Special Ceramics*, P. Popper, ed., British Ceramic Society, Stoke-on-Trent, 1975, vol. 6, pp. 171–81.
9. W. van Rijswijk and D.J. Shanefield: *J. Am. Ceram. Soc.*, 1990, vol. 73, pp. 148–49.
10. W.J. Clegg: *J. Am. Ceram. Soc.*, 2000, vol. 83, pp. 1039–43.
11. F.F. Lange and T.K. Gupta: *J. Am. Ceram. Soc.*, 1976, vol. 59, pp. 537–38.
12. R. Kieffer, E. Gugel, G. Leimer, and P. Ettmayer: *Ber Dt Keram Ges.*, 1972, vol. 49, pp. 41–46.
13. P. Barick, D. Chakravarty, B.P. Saha, R. Mitra, and S.V. Joshi: *Ceram. Inter.*, 2016, vol. 42, pp. 3836–48.
14. A. Malinge, A. Coupe, Y. Petitcorps, and R. Pailler: *J. Euro. Ceram. Soc.*, 2012, vol. 32, pp. 4393–4400.
15. M.S. Datta, A.K. Bandyopadhyay, and B. Cahudhuri: *Bull. Mater. Sci.*, 2002, vol. 25, pp. 181–89.
16. J. Wang and R. Raj: *J. Am. Ceram. Soc.*, 1990, vol. 73, pp. 1172–75.
17. J. Wang and R. Raj: *J. Am. Ceram. Soc.*, 1991, vol. 74, pp. 1959–63.
18. D.A. Ray, S. Kaur, R.A. Cutler, and D.K. Shetty: *J. Am. Ceram. Soc.*, 2008, vol. 91, pp. 1135–40.
19. M.G. Bothara, S.V. Atre, S.J. Park, R.M. German, T.S. Sudarshan, and R. Radhakrishnan: *Metal. Mater. Trans. A.*, 2010, vol. 41A, pp. 3252–61.
20. C. Ziccardi and R. Haber: Addition of Excess Carbon to SiC to Study its Effect on Silicon Carbide (SiC) Armor in *Advances in Ceramic Armor II: Ceram. Eng. Sci. Proc.*, L. Prokurat, A. Wereszczak, and E. Lara-Curzio eds., 2008, vol. 27, pp. 97–103.
21. G. Bernard-Granger and C. Guizard: *J. Am. Ceram. Soc.*, 2007, vol. 90, pp. 1246–50.
22. J.D. Hong and R.F. Davis: *J. Am. Ceram. Soc.*, 1980, vol. 63, pp. 546–52.
23. T.T. Fang, J.T. Shiue, and F.S. Shiau: *Mater. Chem. Phys.*, 2003, vol. 80, pp. 108–13.
24. D.S. Wilkinson and M.F. Ashby: *Acta Mater.*, 1975, vol. 23, pp. 1277–85.
25. R. Hamming, G. Grathwohl, and F. Thummler: *J. Mater. Sci.*, 1983, vol. 18, pp. 3154–60.
26. W.D. Kingery, H.K. Bowen, and R.D. Uhlmann: *Introduction to Ceramics*, 2nd ed., Wiley, New York, 1976.
27. R.N. Ghostagore and R.L. Coble: *Phys. Rev.*, 1966, vol. 143, pp. 623–26.
28. K.M. Friederich and R.L. Coble: *J. Am. Ceram. Soc.*, 1983, vol. 66, pp. C141–42.
29. P.T.B. Shaffer: *Mater. Res. Bull.*, 1970, vol. 5, pp. 519–22.
30. Y. Tajima and W.D. Kingery: *J. Am. Ceram. Soc.*, 1982, vol. 65, pp. C27–29.
31. S.G. Sridhara, L.L. Clemen, R.P. Devaty, W.J. Choyke, D.J. Larkin, H.S. Kong, T. Troffer, and G. Pensl: *J. App. Phys.*, 1998, vol. 83, pp. 7909–19.
32. D.P. Brine: *J. Am. Ceram. Soc.*, 1968, vol. 69, pp. C33–35.
33. S. Grasso, T. Saunders, H. Porwal, and M. Reece: *Ceram. Inter.*, 2015, vol. 14, pp. 225–30.